Title

Molecular imaging of lymphoid organs and immune activation by positron emission tomography with a new [18F]-labeled 2′-deoxycytidine analog

Journal

Nature Medicine, 14(7)

ISSN

1078-8956

Authors

Radu, Caius G
Shu, Chengyi J
Nair-Gill, Evan
et al.

Publication Date

2008-07-01

DOI

10.1038/nm1724

Peer reviewed

HHS Public Access

Author manuscript

Nat Med. Author manuscript; available in PMC 2009 August 03.

Published in final edited form as:

Nat Med. 2008 July ; 14(7): 783–788. doi:10.1038/nm1724.

Molecular imaging of lymphoid organs and immune activation using positron emission tomography with a new ^{18}F-labeled 2′-deoxycytidine analog

Caius G. Radu[1,2], **Chengyi J. Shu**[3], **Evan Nair-Gill**[1], **Stephanie M. Shelly**[1], **Jorge R. Barrio**[1], **Nagichettiar Satyamurthy**[1], **Michael E. Phelps**[1,2], and **Owen N. Witte**[1,3,4]

[1] Department of Molecular and Medical Pharmacology, University of California at Los Angeles (UCLA)

[2] Crump Institute for Molecular Imaging, University of California at Los Angeles (UCLA)

[3] Department of Microbiology, Immunology and Molecular Genetics, David Geffen School of Medicine, University of California at Los Angeles (UCLA)

[4] Howard Hughes Medical Institute at UCLA

Abstract

Monitoring immune function using molecular imaging could significantly impact the diagnosis and treatment evaluation of immunological disorders and therapeutic immune responses. Positron Emission Tomography (PET) is a molecular imaging modality with applications in cancer and other diseases. PET studies of immune function have been limited by a lack of specialized probes. We identified [^{18}F]FAC (1-(2′-deoxy-2′-[^{18}F]fluoroarabinofuranosyl) cytosine) by differential screening as a new PET probe for the deoxyribonucleotide salvage pathway. [^{18}F]FAC enabled visualization of lymphoid organs and was sensitive to localized immune activation in a mouse model of anti-tumor immunity. [^{18}F]FAC microPET also detected early changes in lymphoid mass in systemic autoimmunity and allowed evaluation of immunosuppressive therapy. These data support the use of [^{18}F]FAC PET for immune monitoring and suggest a wide range of clinical applications in immune disorders and in certain types of cancer.

Keywords

FAC (1-(2-deoxy-2-[^{18}F]fluoroarabinofuranosyl) cytosine); deoxyribonucleotide salvage pathway; PET; T lymphocytes; autoimmunity; cancer

Correspondence should be addressed to C.G.R. (cradu@mednet.ucla.edu) or O.N.W. (owenw@microbio.ucla.edu).

Author contributions: C.G.R., C.J.S., E.N.G., N.S., J.R.B., M.E.P. and O.N.W. designed research; C.G.R., C.J.S., E.N.G., N.S. and S.M.S. performed research; C.G.R., C.J.S., E.N.G., N.S., S.M.S. and O.N.W. analyzed data; C.G.R., C.J.S and O.N.W. wrote the paper.

INTRODUCTION

Imaging the immune system in living subjects can define the spatiotemporal programming of innate and adaptive immunity. PET enables noninvasive, quantitative and tomographic assays of biological processes using molecular probes labeled with positron-emitting radioisotopes 1. Studies in mice showed that PET is useful to visualize immune responses. Anti-tumor T cell responses can be monitored by PET reporter gene imaging 2–6. Using a mouse model of autoimmune demyelination we showed that ^{18}Fluorodeoxyglucose ([^{18}F]FDG)1 PET allows imaging of disease onset and of immunosuppressive therapy 7. However, [^{18}F]FDG accumulation in tissues like heart, brain and liver suggests the need for new PET probes with distinct biodistribution patterns. To develop such probes, we focused on the salvage pathway for DNA synthesis in which deoxyribonucleosides are converted to nucleotides by phosphorylation catalyzed by deoxyribonucleoside kinases (reviewed in 8). While most tissues predominantly utilize the *de novo* pathway for DNA synthesis, lymphoid organs and rapidly proliferating tissues rely extensively on the salvage pathway 9. To identify novel probes for the salvage pathway we: (*i*), *in vitro* screened nucleoside analogs for differential retention in proliferating and quiescent T cells; (*ii*), identified FAC, a new PET probe candidate with increased accumulation in proliferating T cells; (*iii*), performed gene expression and biochemical analyses to investigate the mechanism(s) of elevated FAC retention; (*iv*), radiochemically synthesized [^{18}F]FAC for *in vivo* biodistribution studies; (*v*), compared [^{18}F]FAC with PET probes currently used to measure nucleoside metabolism and glycolysis; and (*vi*), evaluated [^{18}F]FAC in mouse models of immune activation. Similar strategies are broadly applicable to the development of new PET probes with specificity for various biochemical pathways and/or immune cell lineages. Our findings provide the impetus for clinical evaluation of [^{18}F]FAC PET imaging in immune disorders and other diseases.

RESULTS

Differential screening to identify potential PET probes sensitive to changes in nucleoside flux associated with T cell activation and proliferation

We measured the retention of [^{3}H]-labeled deoxyribonucleoside analogs (NAs) in resting vs. proliferating primary CD8^{+}T cells. Selection criteria for NAs accounted for the propensity of fluorine substitutions to change the biochemical properties of nucleosides (reviewed in 10). Since fluorination at C-4′ is incompatible with ^{18}F labeling and fluorination at C-5′ would prevent phosphorylation by nucleoside kinases, we tested only NAs containing ‘cold’ fluorine (^{19}F) atom(s) substitutions at C-2′ or 3′ on the sugar moiety or at position 5 of the nucleobase (Supplementary Fig. 1 online). Fig. 1a shows a wide variation in NAs retention by quiescent and proliferating CD8^{+} T cells. While 2′,2′-difluorodeoxycytidine (dFdC) (Fig. 1b) showed the best selectivity for proliferating cells, synthesis of ^{18}F-labeled dFdC would be challenging. Precursors for [^{18}F]dFdC are likely to be unstable because of the presence of the electronegative fluorine atom and an excellent leaving group at the C-2′ position. This and the need for large mass of precursor materials limit the specific activity of [^{18}F]dFdC. To circumvent this problem we synthesized ^{18}F labeled monofluorinated analogs of dFdC (Supplementary Fig. 2 online). Relative to the stereochemical configurations of the C-2′

fluorine atom (Fig. 1b), the F-*ara* ('up') analogs retain biological activity while the C-2′ *ribo* ('down') compounds are inactive (reviewed in 10). Indeed, similar amounts of the F-*ara* analog 1-(2- deoxy-2-fluoro-arabinofuranosyl)-cytosine (FAC) (Fig. 1b) and dFdC were retained in proliferating $CD8^+$ T cells (Fig. 1c). FAC retention in dividing T cells could reflect any one or combination of several biochemical events: (*i*), upregulation of nucleoside transporters; (*ii*), elevated phosphorylation by deoxyribonucleoside kinases; and, (*iii*), increased incorporation into the DNA. To determine expression of nucleoside transporters and kinases potentially involved in FAC retention we performed microarray and qPCR analyses. 2′-deoxycytidine (dCyd) analogs are transported by members of the solute carrier (SLC) families SLC28 (reviewed in 11) and SLC29 (reviewed in 12). *Slc29a1* expression was upregulated by ~4-fold in proliferating T cells vs. quiescent T cells while *Slc28a1* and *Slc28a3* 11 were not expressed (data not shown). Intracellular FAC could be phosphorylated and trapped by deoxycytidine kinase (dCK, K_{cat}/K_m for dCyd = 2×10^5) and by thymidine kinase 2 (TK2, K_{cat}/K_m for dCyd = 3×10^4) (reviewed in 13). Following T cell activation, dCK mRNA levels increased by ~2-fold whereas TK2 expression decreased by ~5-fold (data not shown). Since SLC29A1 and dCK were previously involved in the metabolism of dFdC 14,15, we further analyzed their role by overexpressing them in NIH3T3 fibroblasts. Thymidine kinase 1 (TK1, K_{cat}/K_m for dCyd $<1 \times 10^2$ 13) was used as a negative control. [^{3}H]FAC retention increased in both dCK^{HIGH} and $SLC29A1^{HIGH}$ cells but not in $TK1^{HIGH}$ cells which only accumulated [^{3}H]fluorothymidine (FLT) (Fig. 1d). To determine whether retention could also reflect DNA incorporation, T cells were activated for 72 hrs and then incubated for 1 to 8 hrs with [^{3}H]FAC. The accumulation of [^{3}H]FAC and [^{3}H]dCyd (positive control) into DNA increased as a function of time (Fig. 1e).

[^{18}F]FAC has greater specificity for lymphoid organs than PET probes for nucleoside metabolism and glycolysis

Radiochemical synthesis of [^{18}F]FAC (Supplementary Fig. 2 online) reproducibly yielded a product with chemical and radiochemical purities greater than 99% and specific activity greater than 1 Ci/μmol. HPLC analysis of [^{18}F]FAC up to 10 hrs post radiochemical synthesis did not detect products of radiolysis. Biodistribution, metabolism and clearance of [^{18}F]FAC were studied in C57/BL6 mice. Tissue decay-corrected mean time-activity curves from dynamic [^{18}F]FAC microPET/CT scans (Supplementary Fig. 3a online) suggested that [^{18}F]FAC was predominantly cleared through kidney and liver (Supplementary Fig. 3a,b online). Imaging data were corroborated with radioactivity measurements in necropsy tissue samples (Supplementary Fig. 3c online) and with digital whole-body autoradiography (DWBA) (Fig. 2a). One hour after injection of [^{18}F]FAC, accumulated radioactivity was detected in thymus, spleen, intestine, bone/bone-marrow and liver. Similar to other deoxycytidine analogs, FAC is susceptible to deamination *in vivo* 16 (Supplementary Fig. 4 online). Two lines of evidence suggest that the tissue accumulation of [^{18}F]FAC is primarily regulated by dCK-mediated phosphorylation rather than by deamination. First, [^{18}F]FAC and its phosphorylated derivatives was detected by HPLC analyses of thymic extracts. Second, biodistribution data indicated preferential retention of [^{18}F]FAC in tissues with high dCK mRNA expression 13. While further studies are required to precisely define biochemical mechanism(s) of retention, our data suggested that [^{18}F]FAC enables

visualization of cells with high deoxyribonucleoside salvage 9 such as lymphocytes, bone-marrow cells and enterocytes.

Compared with probes for nucleoside metabolism ([^{18}F]FLT 17 and [^{18}F]D-FMAU 18) and glycolysis ([^{18}F]FDG), [^{18}F]FAC had a distinct biodistribution pattern (Fig. 2c, Table 1, Supplementary Fig. 5 online). [^{18}F]FLT and [^{18}F]D-FMAU showed no detectable accumulation in thymus and spleen while myocardial retention of [^{18}F]FDG interferes with the thymus signal. To examine the cell lineage specificity of [^{18}F]FAC resident populations from thymus and spleen were sorted using flow cytometry. While rapidly dividing double negative thymocytes had the highest retention of radioactivity, [^{18}F]FAC also labeled peripheral T and B lymphocytes as well as CD11b^{+} myeloid cells (Fig. 2d,e).

[^{18}F]FAC microPET imaging of immune activation during a primary anti-tumor immune response

To determine whether [^{18}F]FAC is sensitive to localized immune activation we used a onco-retrovirus tumor model 19 characterized by T cell priming by strong xenoantigens encoded by the *gag* and *env* genes of the Moloney murine sarcoma and leukemia virus complex (MoMSV). As shown using conventional *ex vivo* approaches 20 and PET reporter gene imaging 3,6, non-metastatic MoMSV induced sarcomas are rejected in a T-cell dependent manner with reproducible kinetics. [^{18}F]FAC scans at the peak of the anti-tumor immune response (Day 15) Fig. 3a,b, Supplementary Fig. 6 online) indicated increased accumulation in the spleen and tumor draining lymph nodes (DLNs) relative to Day -1 baseline scans. We then examined whether elevated retention of [^{18}F]FAC at these sites reflects upregulated nucleoside salvage metabolism by activated CD8^{+} T cells. Splenic CD8^{+} T cells from mice injected with [^{18}F]FAC were fractionated by flow cytometry into naïve (CD62L^{HIGH}/CD44^{LOW}) and effector populations (CD62L^{LOW}/CD44^{HIGH}). Effector CD8^{+} T cells retained ~4-fold more [^{18}F]FAC than naïve T cells (Fig. 3c).

To compare [^{18}F]FAC with other probes MoMSV-challenged mice were scanned on consecutive days with [^{18}F]FAC, [^{18}F]FDG and [^{18}F]FLT. On Day 13 post virus challenge, [^{18}F]FDG accumulation was increased at the tumor site, tumor DLNs and spleen (Fig. 3d and Supplementary Fig. 6 online). Tumor lesions accumulated high amounts of [^{18}F]FDG: 8.2 ±4.2 percent injected dose of activity per gram of tissue (%ID/g) of tumor over background (defined as the contralateral muscle tissue). In contrast, [^{18}F]FAC retention in the tumor was lower (1.9 ±0.3 %ID/g). Although additional studies are required to elucidate whether [^{18}F]FAC retention in tumors is due to infiltrating immune cells, preferential accumulation in the tumor DLNs (4.14 ±1.5 %ID/g) vs. tumor (1.9 ±0.3 %ID/g) (Fig. 3a,d, Supplementary Fig. 6 online) suggested that [^{18}F]FAC has good specificity for imaging immune rejection of virally-induced sarcomas. In contrast to [^{18}F]FAC, [^{18}F]FLT did not accumulate at sites of immune activation (Fig. 3e).

Disease and treatment evaluation using [^{18}F]FAC PET in an animal model of systemic autoimmunity

To determine whether [^{18}F]FAC could allow monitoring of autoimmune disorders we used mice carrying the Fas^{lpr} mutation. Deficient apoptosis of Fas^{lpr} lymphocytes leads to

lymphadenopathy, arthritis and immune complex-mediated glomerulonephrosis 21. We used B6.MRL-*Fas*^{lpr}/J mice which show slower disease progression than the MRL/Mp-*lpr/lpr* strain 22. PET/CT scans of 2-3 month old B6.MRL-*Fas*^{lpr}/J mice revealed increased numbers of [^{18}F]FAC positive axillary and brachial lymph nodes (LNs) relative to age-matched wild type (WT) C57BL/6J controls (Fig. 4, Supplementary Fig. 7a online). [^{18}F]FAC positive LNs could be detected in 2 of 19 WT mice, whereas 9 of 13 *Fas*^{lpr}/J mice showed signals indicative of lymphadenopathy. Quantification of [^{18}F]FAC accumulation in LNs from *Fas*^{lpr}/J mice showed an excellent correlation between retained radioactivity and T cell numbers (Supplementary Fig. 7b online). To determine whether [^{18}F]FAC microPET/CT could monitor therapy, B6.MRL-*Fas*^{lpr}/J mice were given dexamethasone (DEX), a synthetic glucocorticoid with potent immunosuppressive effects 23. DEX had a profound effect on [^{18}F]FAC retention in thymus and LNs presumably reflecting the cytotoxic effects of this drug towards lymphocytes (Fig. 4, Supplementary Fig. 7a online).

DISCUSSION

A new PET probe for imaging the immune system

[^{18}F]FAC is a novel PET probe which allows visualization of thymus and spleen in mice and is sensitive to alterations in lymphoid mass and immune status. Current results and our previous [^{18}F]FDG PET imaging study in Experimental Autoimmune Encephalomyelitis (EAE)7 indicate that [^{18}F]FAC and [^{18}F]FDG can be used to measure key metabolic pathways in immune cells. While these probes are not absolutely specific for immune cells, changes in their accumulation throughout the body could be indicative of “disease states” and could provide early biomarkers. Direct comparisons of [^{18}F]FAC with [^{18}F]FDG and [^{18}F]FLT indicate that [^{18}F]FAC has better selectivity for lymphoid organs such as thymus, spleen and lymph nodes. Potential disadvantages of [^{18}F]FAC include its baseline retention in lymphoid organs which could hamper the detection of weak immune responses at these sites and relatively high retention in the small and large intestine.

[^{18}F]FAC as a cancer imaging probe

Dysregulated nucleoside metabolism represents a hallmark of cancer and preliminary results indicate that [^{18}F]FAC could be useful in oncology imaging. We evaluated [^{18}F]FAC in several tumor models (Supplementary Fig. 8 online). Increased [^{18}F]FAC retention in the spleen was observed in leukemia induced by transplantation of Bcr-Abl transformed Ba/F3 cells or bone marrow cells. [^{18}F]FAC PET visualized tumors induced by murine B16 cells (representative of malignant melanoma) and human U87 cells (representative of glioma tumors). Future studies are warranted to directly compare [^{18}F]FAC with [^{18}F]FDG and [^{18}F]FLT for detection of various cancers. Furthermore, [^{18}F]FAC PET could enable prediction of tumor responses to a class of anticancer agents represented by structurally related prodrugs cytarabine (Ara-C) and 2′-difluorodeoxycytidine (dFdC, Gemcitabine). Similar to FAC retention, the activation of these widely used prodrugs requires uptake via similar nucleoside transporters and dCK-mediated phosphorylation (reviewed in 13).

In conclusion, [^{18}F]FAC PET imaging could offer new insights for diagnostics and treatment monitoring of a wide range of disorders. Studies are underway to translate

[^{18}F]FAC PET imaging to the clinic and evaluate its potential for monitoring autoimmunity, inflammation and cancer.

METHODS

[^{3}H]-labeled nucleosides (see also Supplementary Fig. 1)

The following tritium labeled nucleosides were purchased from Moravek Biochemicals (Brea, CA): 3′ Fluoro 3′ deoxythymidine (3′FLT); 2′ Fluoro 2′ deoxy-Thymidine (2′FLT); 1-(2-Deoxy-2-Fluoro-B-D-arabino-furanosyl)-5-methyluracil (D-FMAU); 1-(2-Deoxy-2-Fluoro-B-L-arabinofuranosyl) 5 methyluracil (L-FMAU); 2,3-dideoxy-3-fluorocytidine (3′FddC); (-)-β-2,3-Dideoxy-5-fluoro-3-thiacytidine (FTC); 5-Fluoro-2,3-dideoxycytidine (5FddC); 2′,2′-Difluorodeoxycytidine (dFdC); 5-Fluoro-2′-Deoxycytidine (5FdC); 5-Fluoro-2-deoxyuridine (5FdURD); 2′-Fluoro-2-deoxyuridine (2FdUrd); 1-(2-deoxy-2-fluoro-B-D-arabinofuranosyl)-uracil (FAU); 2′-Fluoro-2′-deoxy5-Fluorouracil-β-D—arabino-furanoside (FFAU).

T cell activation and radioactive tracer uptake assay

T lymphocytes from pmel-1 T cell receptor (TCR) transgenic mice 24 were stimulated *ex vivo* using their cognate antigen (1 μM hgp100$_{25–33}$) and cultured for 72 hrs. For radioactive tracer uptake assays, 1 μCi of [^{3}H]FAC or [^{3}H]dFdC were added to wells containing 5x10^{4} cells in a 96-well tissue culture plate and incubated for 1 hr at 37^{o}C and 5% CO_2. The plate was washed five times with media containing 5% fetal calf serum using the Millipore Vacuum Manifold (Billerica, MA). The amount of incorporated probe was measured by scintillation counting using the PerkinElmer Microbeta (Waltham, MA). DNA incorporation assays using [^{3}H]-labeled nucleosides were performed as previously described 25.

Radiochemical synthesis of ^{18}F-labeled PET probes

The radiochemical synthesis of [^{18}F]FAC is described in Supplementary Fig. 2 online. The radiochemical synthesis of [^{18}F]FDG 26, [^{18}F]FLT 17, and [^{18}F]D-FMAU 27 was performed as previously described.

MicroPET/CT imaging

Mice were kept warm under gas anesthesia (2% isoflurane) and injected with 200 μCi of various PET probes i.v. and allowed 1 hr uptake. Mice were then positioned using an imaging chamber. Data were acquired using Siemens Preclinical Solutions (Knoxville, TN) microPET Focus 220 and MicroCAT II CT systems. MicroPET data were acquired for 10 minutes and reconstructed using a statistical maximum a posteriori probability algorithm (MAP) 28 into multiple frames. The spatial resolution of PET is ~1.5 mm, 0.4 mm voxel size. CT images are a low dose 400 μm resolution acquisition with 200 μm voxel size. MicroPET and CT images were co-registered as previously described 29. Quantification was performed by drawing 3D regions of interest (ROI) using the AMIDE software 30. Color scale is proportional to tissue concentration with red being the highest and lower values in yellow, green & blue.

Animal models for immune activation

Mice used in these studies were bred and maintained according to the guidelines of the Department of Laboratory Animal Medicine (DLAM) at the University of California, Los Angeles. The MoMSV sarcoma model was described previously 3. B6.MRL-Fas^{lpr}/J mice used for systemic autoimmunity studies were purchased from The Jackson Laboratory (stock number: 000482). Dexamethasone (DEX, 10 mg/kg) was administered by intraperitoneal injections in 100 μL PBS at 24 hr intervals for 2-7 days. Mice were scanned by microPET/CT 24 hr after the last injection.

Digital whole-body autoradiography

Mice were anesthetized with 2% isoflurane and were injected i.v. with 1mCi [^{18}F]FAC. The DWBA was performed by using previously described methods 7. Frozen coronal whole body mouse sections (45 μm thick) were exposed overnight and were developed using a Fuji BAS 5000 Imager at 100 μm spatial resolution.

Data presentation and statistical analysis

Graphs were constructed using GraphPad Prism software, version 4.02. *P* values were calculated using Student's *t* test. *P* values of <0.05 were considered significant. Data are presented as means ± standard errors of the mean (SEM).

Supplementary Material

Refer to Web version on PubMed Central for supplementary material.

Acknowledgments

We are grateful to D. Stout, W. Ladno and J. Edwards for microPET imaging, the chemists and cyclotron group for production of PET probes. We thank G. Toy, M. Riedinger, S. Quan, D. Chen, J. Wengrod, D. Goldstein and A. Tran for outstanding technical assistance. We thank J. Lee for the analysis of the microarray data, Helen Su for imaging the U87 tumors, J. Liu and C. Shen for help with biochemical analyses, Jami McLaughlin for providing leukemic animal models for imaging studies and J. Czernin, H. Herschman and A. Ribas for insightful discussions. We also thank B. Anderson for help with preparing the manuscript. O.N.W. is an Investigator of the Howard Hughes Medical Institute. C.G.R. was supported by *In Vivo* Cellular and Molecular Imaging Centers (ICMIC) Developmental Project Award NIH P50 CA86306 from the National Cancer Institute, National Institutes of Health, by a National Cancer Institute Grant No. 5U54 CA119347 and by a JDRF Award #17-2006-870 (O.N.W.). C.G.R. acknowledges unrestricted support from Merck Research Laboratories. C.J.S. was supported by a Fred Eiserling and Judith Lengyel Graduate Doctorate Fellowship. E.N.G. was supported by the MSTP program NIH Grant #T32 GM08042. This research was supported in part by U.S. Department of Energy Contract DE-FG02-06ER64249 (M.E.P.) and by National Cancer Institute Grant R24CA92865.

Abbreviations

PET	positron emission tomography
CT	computed tomography
NAs	nucleoside analogs
[^{18}F]FAC	1-(2-deoxy-2-[^{18}F]fluoroarabinofuranosyl) cytosine
dFdC	2′,2′-Difluorodeoxycytidine

[^{18}F]FLT	3′-deoxy-3′-[^{18}F]fluorothymidine
[^{18}F]FDG	2-[^{18}F] fluoro-2-deoxy-D-glucose
[^{18}F]D-FMAU	2′-[^{18}F]fluoro-5 Methylarabinosyluracil
dCK	deoxycytidine kinase
SLC	solute carrier gene transporter
ROI	region of interest
%ID/g	percent injected dose per gram of tissue
DEX	dexamethasone

References

1. Phelps ME. Inaugural article: positron emission tomography provides molecular imaging of biological processes. Proceedings of the National Academy of Sciences of the United States of America. 2000; 97:9226–9233. [PubMed: 10922074]
2. Koehne G, et al. Serial in vivo imaging of the targeted migration of human HSV-TK-transduced antigen-specific lymphocytes. Nature biotechnology. 2003; 21:405–413.
3. Dubey P, et al. Quantitative imaging of the T cell antitumor response by positron-emission tomography. Proc Natl Acad Sci U S A. 2003; 100:1232–1237. [PubMed: 12547911]
4. Su H, Forbes A, Gambhir SS, Braun J. Quantitation of cell number by a positron emission tomography reporter gene strategy. Mol Imaging Biol. 2004; 6:139–48. [PubMed: 15193248]
5. Shu CJ, et al. Visualization of a primary anti-tumor immune response by positron emission tomography. Proc Natl Acad Sci U S A. 2005; 102:17412–17417. [PubMed: 16293690]
6. Su H, Chang DS, Gambhir SS, Braun J. Monitoring the antitumor response of naive and memory CD8 T cells in RAG1−/− mice by positron-emission tomography. J Immunol. 2006; 176:4459–4467. [PubMed: 16547284]
7. Radu CG, Shu CJ, Shelly SM, Phelps ME, Witte ON. Positron emission tomography with computed tomography imaging of neuroinflammation in experimental autoimmune encephalomyelitis. Proc Natl Acad Sci U S A. 2007; 104:1937–1942. [PubMed: 17261805]
8. Van Rompay AR, Johansson M, Karlsson A. Substrate specificity and phosphorylation of antiviral and anticancer nucleoside analogues by human deoxyribonucleoside kinases and ribonucleoside kinases. Pharmacology & therapeutics. 2003; 100:119–139. [PubMed: 14609716]
9. Griffith DA, Jarvis SM. Nucleoside and nucleobase transport systems of mammalian cells. Biochimica et biophysica acta. 1996; 1286:153–181. [PubMed: 8982282]
10. Pankiewicz KW. Fluorinated nucleosides. Carbohydrate research. 2000; 327:87–105. [PubMed: 10968677]
11. Gray JH, Owen RP, Giacomini KM. The concentrative nucleoside transporter family, SLC28. Pflugers Arch. 2004; 447:728–734. [PubMed: 12856181]
12. Baldwin SA, et al. The equilibrative nucleoside transporter family, SLC29. Pflugers Arch. 2004; 447:735–743. [PubMed: 12838422]
13. Eriksson S, Munch-Petersen B, Johansson K, Eklund H. Structure and function of cellular deoxyribonucleoside kinases. Cell Mol Life Sci. 2002; 59:1327–1346. [PubMed: 12363036]
14. Nakano Y, et al. Gemcitabine chemoresistance and molecular markers associated with gemcitabine transport and metabolism in human pancreatic cancer cells. British journal of cancer. 2007; 96:457–463. [PubMed: 17224927]
15. van der Wilt CL, et al. The role of deoxycytidine kinase in gemcitabine cytotoxicity. Advances in experimental medicine and biology. 2000; 486:287–290. [PubMed: 11783501]

16. Shipley LA, et al. Metabolism and disposition of gemcitabine, and oncolytic deoxycytidine analog, in mice, rats, and dogs. Drug metabolism and disposition: the biological fate of chemicals. 1992; 20:849–855. [PubMed: 1362937]
17. Shields AF, et al. Imaging proliferation in vivo with [F-18]FLT and positron emission tomography. Nature medicine. 1998; 4:1334–1336.
18. Sun H, et al. Imaging DNA synthesis in vivo with 18F-FMAU and PET. J Nucl Med. 2005; 46:292–296. [PubMed: 15695789]
19. Fefer A, McCoy JL, Perk K, Glynn JP. Immunologic, virologic, and pathologic studies of regression of autochthonous Moloney sarcoma virus-induced tumors in mice. Cancer research. 1968; 28:1577–1585. [PubMed: 4876979]
20. Schepers K, et al. Differential kinetics of antigen-specific CD4+ and CD8+ T cell responses in the regression of retrovirus-induced sarcomas. J Immunol. 2002; 169:3191–3199. [PubMed: 12218137]
21. Morse HC 3rd, et al. Abnormalities induced by the mutant gene Ipr: expansion of a unique lymphocyte subset. J Immunol. 1982; 129:2612–2615. [PubMed: 6815273]
22. Kelley VE, Roths JB. Interaction of mutant lpr gene with background strain influences renal disease. Clinical immunology and immunopathology. 1985; 37:220–229. [PubMed: 4042431]
23. McKay LI, Cidlowski JA. Molecular control of immune/inflammatory responses: interactions between nuclear factor-kappa B and steroid receptor-signaling pathways. Endocrine reviews. 1999; 20:435–459. [PubMed: 10453354]
24. Overwijk WW, et al. Tumor regression and autoimmunity after reversal of a functionally tolerant state of self-reactive CD8+ T cells. The Journal of experimental medicine. 2003; 198:569–580. [PubMed: 12925674]
25. Le LQ, et al. Mice lacking the orphan G protein-coupled receptor G2A develop a late-onset autoimmune syndrome. Immunity. 2001; 14:561–571. [PubMed: 11371358]
26. Hamacher K, Coenen HH, Stocklin G. Efficient stereospecific synthesis of no-carrier-added 2-[18F]-fluoro-2-deoxy-D-glucose using aminopolyether supported nucleophilic substitution. J Nucl Med. 1986; 27:235–238. [PubMed: 3712040]
27. Mangner TJ, Klecker RW, Anderson L, Shields AF. Synthesis of 2′-deoxy-2′-[18F]fluoro-beta-D-arabinofuranosyl nucleosides, [18F]FAU, [18F]FMAU, [18F]FBAU and [18F]FIAU, as potential PET agents for imaging cellular proliferation. Synthesis of [18F]labelled FAU, FMAU, FBAU, FIAU. Nuclear medicine and biology. 2003; 30:215–224. [PubMed: 12745012]
28. Qi J, Leahy RM, Cherry SR, Chatziioannou A, Farquhar TH. High-resolution 3D Bayesian image reconstruction using the microPET small-animal scanner. Phys Med Biol. 1998; 43:1001–1013. [PubMed: 9572523]
29. Chow PL, Stout DB, Komisopoulou E, Chatziioannou AF. A method of image registration for small animal, multi-modality imaging. Phys Med Biol. 2006; 51:379–390. [PubMed: 16394345]
30. Loening AM, Gambhir SS. AMIDE: a free software tool for multimodality medical image analysis. Mol Imaging. 2003; 2:131–137. [PubMed: 14649056]

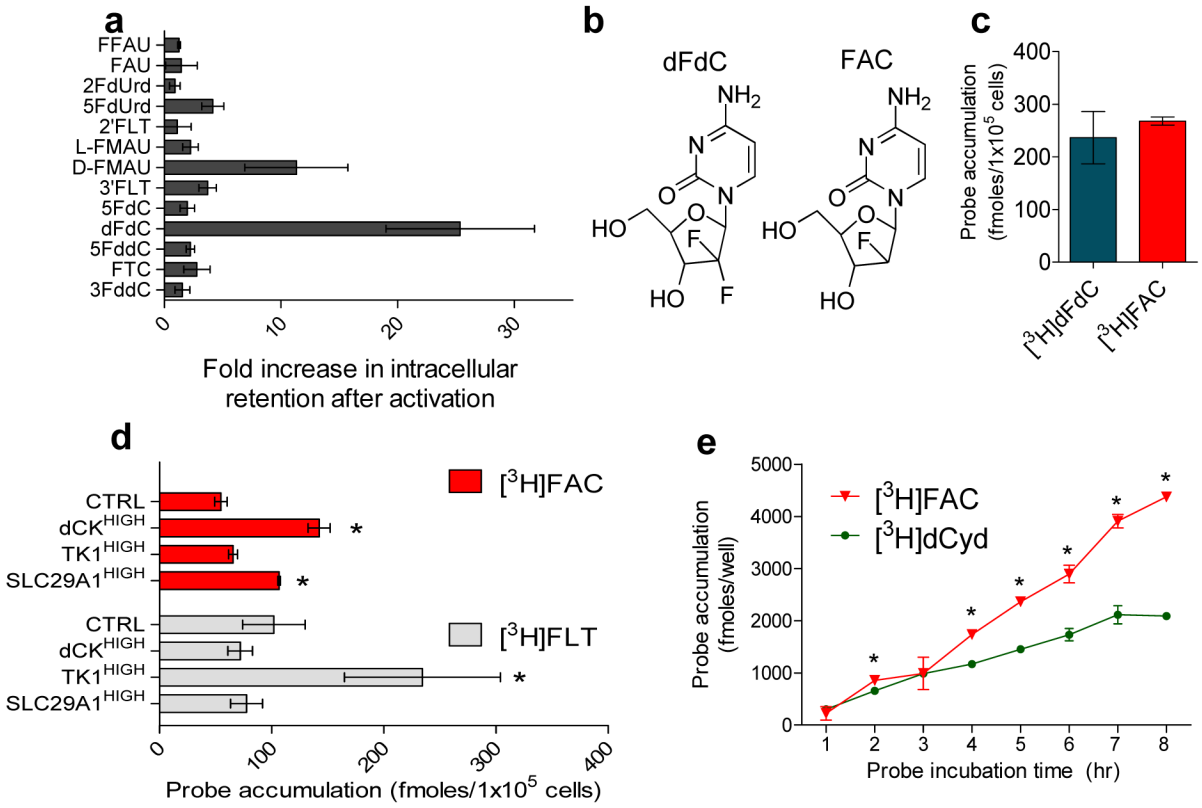

Figure 1. Identification of fluorinated deoxycytidine analogs retained in activated vs. naïve T cells

(a) Primary CD8$^+$ T cells were stimulated *ex vivo* for 72 hrs and then were incubated for 1 hr with [^{3}H]-labeled NAs; following successive washes, intracellular radioactivity was measured by scintillation counting. **(b)** FAC is a dFdC analog amenable to ^{18}F labeling. **(c)** Similar retention of [^{3}H]dFdC and [^{3}H]FAC by activated mouse CD8+ T cells; the retention of [^{3}H]FAC in naïve CD8+ T cells was 18+/−4.5 fmoles/10^5 cells **(d)** Increased uptake of [^{3}H]FAC in NIH3T3 fibroblasts engineered to overexpress nucleoside kinases (dCK, TK1) and the nucleoside transporter SLC29A1. [^{3}H]FLT was used as a positive control for TK1 expressing cells. **(e)** [^{3}H]FAC and the parental nucleoside 2′ deoxycytidine ([^{3}H]dCyd, used as a positive control) are incorporated in the DNA of proliferating CD8+ T cells as a function of time (see text for details). * *P* values of <0.05. Results are representative of two independent experiments.

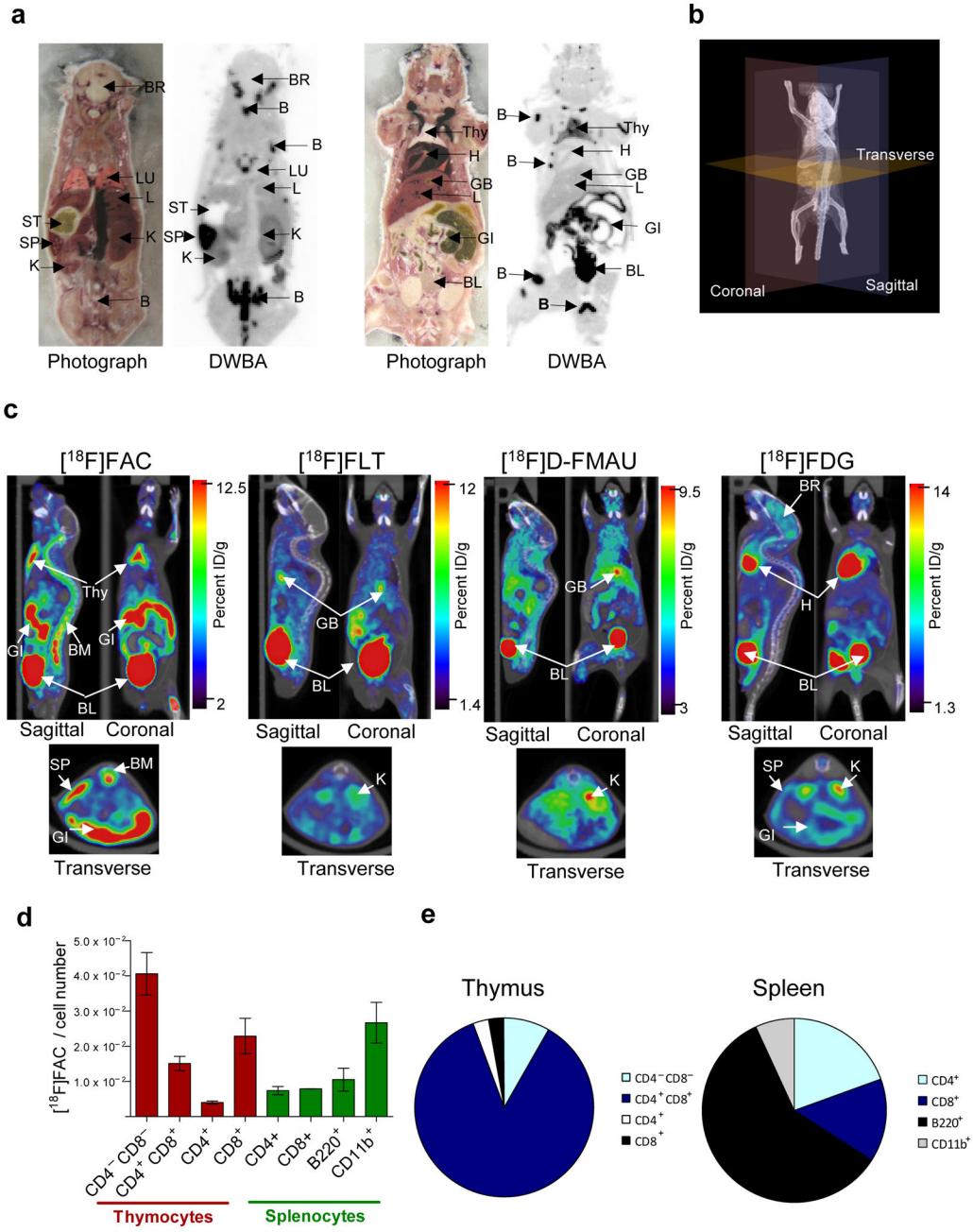

Figure 2. [^{18}F]FAC has better selectivity for lymphoid organs compared with other PET probes for nucleoside metabolism and glycolysis

(a) [^{18}F]FAC DWBA shown along with the corresponding tissue sections. **(b,c)** C57/BL6 mice were scanned by microPET/CT using [^{18}F]FAC, [^{18}F]FLT, [^{18}F]D-FMAU and [^{18}F]FDG. Mice were imaged 60 min after i.v. injection of probes. The orientation of saggital, coronal and transverse sections is depicted in the 3D microCT image in panel **b**. Images are 1 mm thick sagittal, coronal and transverse slices. Percent ID/g, percent injected dose per gram of tissue; B, Bone; BL, Bladder; BR, Brain; GB, Gall Bladder; GI, Gastrointestinal tract; H, heart; K, Kidney; L, Liver; LU, Lung; SP, Spleen; Thy, thymus;

BM, bone marrow; ST, stomach. **(d)** [^{18}F]FAC retention/cell number in thymocytes and splenocytes. **(d)** Proportion of [^{18}F]FAC retention/cell lineage per lymphoid organ (see text for details).

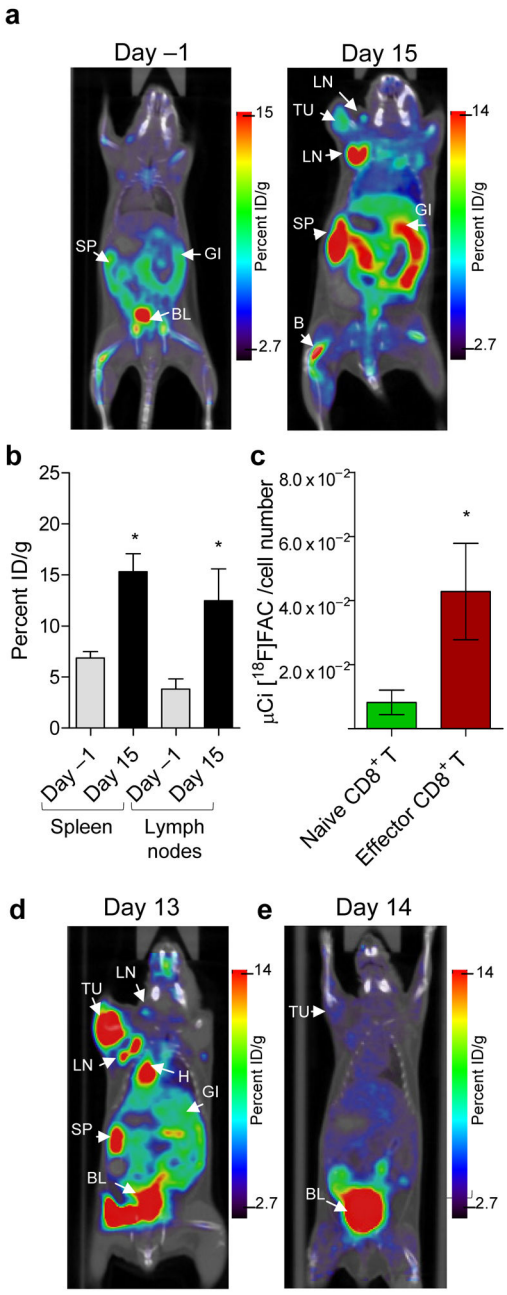

Figure 3. Increased [^{18}F]FAC retention in spleen and lymph nodes at the peak of the primary anti-tumor immune response

Images are 1 mm coronal sections from microPET/CT scans using [^{18}F]FAC (Day -1 and Day 15, panel **a**), [^{18}F]FDG (Day 13, panel **d**) and [^{18}F]FLT (Day 14, panel **e**). B, Bone; BL, Bladder; GI, Gastrointestinal tract; H, heart; SP, Spleen; TU, tumor; Thy, thymus; LN, lymph node. **(b)** Quantification of [^{18}F]FAC retention in spleen and lymph nodes on Day -1 and Day 15; Number of mice =3. **(c)** Increased *in vivo* accumulation of [^{18}F]FAC in effector CD8+ T cells vs. naïve CD8+ T cells. Mice were challenged with the MoMSV onco-retrovirus and 14 days later were injected with 1 mCi [^{18}F]FAC. Following 1 hr *in vivo*

uptake, mice were sacrificed to isolate splenocytes which were fractionated by flow cytometry into naïve $CD8^+$ T cells ($CD44^{LOW}/CD62L^{HIGH}$) and effector $CD8^+$ T cells ($CD44^{HIGH}/CD62L^{LOW}$). Radioactivity accumulated by these cells was measured using a well counter. Results are representative of two independent experiments.

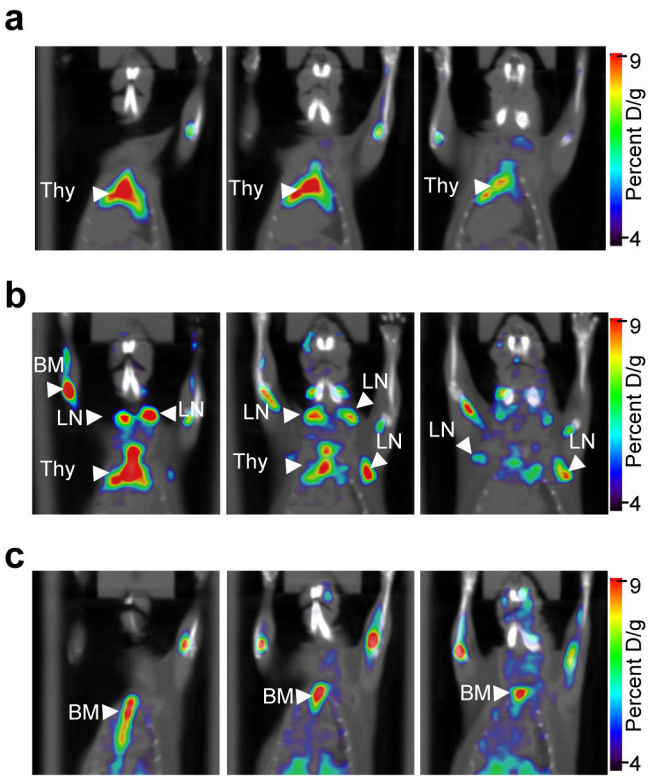

Figure 4. [^{18}F]FAC microPET/CT allows visualization of increased lymphoid mass in systemic autoimmunity and can be used to monitor immunosuppressive therapeutic interventions

Images are 60 minutes after i.v. injection of [^{18}F]FAC and show three 1 mm thick coronal slices from (**a**) wild-type (C57BL/6J) and B6.MRL-*Fas*^{lpr}/J (**b**) before and (**c**) after treatment with DEX. [^{18}F]FAC positive LNs were scored blindly. Thy, thymus; LN, lymph nodes; BM, bone-marrow. Results are representative of two independent experiments.

Table 1

Amongst existing PET probes for nucleoside metabolic pathways and glycolysis, [^{18}F]FAC shows better selectivity for thymus and spleen (values are %ID/g per organ normalized to %ID/g muscle). Retention of [^{18}F]FDG in the thymus could not be measured because of signal spillover from the heart. Number of mice = 3.

	[^{18}F]FAC	[^{18}F]FLT	[^{18}F]FMAU	[^{18}F]FDG
Spleen	2.16+/− 0.48	1.02+/− 0.21	1.08+/− 0.27	1.69+/− 0.16
Thymus	3.29+/− 0.48	1.22+/− 0.23	1.33+/− 0.24	N.D.